

STM study of selenium adsorption on Au(111) surface

Bin Liu(刘斌), Yuan Zhuang(庄源), Yande Que(阙炎德), Chaoqiang Xu(徐超强), Xudong Xiao(肖旭东)
Citation: Chin. Phys. B . 2020, 29(5): 056801 . **doi:** 10.1088/1674-1056/ab821d
Journal homepage: http://cpb.iphy.ac.cn; http://iopscience.iop.org/cpb

What follows is a list of articles you may be interested in

Real-space observation on standing configurations of phenylacetylene on Cu (111) by scanning probe microscopy

Jing Qi(戚竞), Yi-Xuan Gao(高艺璇), Li Huang(黄立), Xiao Lin(林晓), Jia-Jia Dong(董佳家), Shi-Xuan Du(杜世萱), Hong-Jun Gao(高鸿钧)
Chin. Phys. B . 2019, 28(6): 066801 . **doi:** 10.1088/1674-1056/28/6/066801

Epitaxial fabrication of two-dimensional $TiTe_2$ monolayer on Au(111) substrate with Te as buffer layer

Zhipeng Song(宋志朋), Bao Lei(雷宝), Yun Cao(曹云), Jing Qi(戚竞), Hao Peng(彭浩), Qin Wang(汪琴), Li Huang(黄立), Hongliang Lu(路红亮), Xiao Lin(林晓), Ye-Liang Wang(王业亮), Shixuan Du(杜世萱), Hong-Jun Gao(高鸿钧)
Chin. Phys. B . 2019, 28(5): 056801 . **doi:** 10.1088/1674-1056/28/5/056801

Interaction of two symmetric monovacancy defects in graphene

Wen-Yan Xu(徐文焱), Li-Zhi Zhang(张礼智), Li Huang(黄立), Yan-De Que(阙炎德), Ye-Liang Wang(王业亮), Xiao Lin(林晓), Shi-Xuan Du(杜世萱)
Chin. Phys. B . 2019, 28(4): 046801 . **doi:** 10.1088/1674-1056/28/4/046801

Pits and adatoms at the interface of 1-ML C_{84}/Ag (111)

Wang Peng, Zhang Han-Jie, Li Yan-Jun, Sheng Chun-Qi, Li Wen-Jie, Xing Xiu-Na, Li Hai-Yang, He Pi-Mo, Bao Shi-Ning, Li Hong-Nian
Chin. Phys. B . 2013, 22(12): 126803 . **doi:** 10.1088/1674-1056/22/12/126803

One-dimensional diffusion of vacancies on Sr/Si(100)-c(2×4) surface

Yang Jing-Jing, Du Wen-Han
Chin. Phys. B . 2013, 22(6): 066801 . **doi:** 10.1088/1674-1056/22/6/066801

STM study of selenium adsorption on Au(111) surface*

Bin Liu(刘斌), Yuan Zhuang(庄源), Yande Que(阙炎德)†,
Chaoqiang Xu(徐超强), and Xudong Xiao(肖旭东)‡

Department of Physics, the Chinese University of Hong Kong, Shatin, Hong Kong, China

(Received 20 February 2020; revised manuscript received 12 March 2020; accepted manuscript online 23 March 2020)

Adsorption of chalcogen atoms on metal surfaces has attracted increasing interest for both the fundamental research and industrial applications. Here, we report a systematic study of selenium (Se) adsorption on Au(111) at varies substrate temperatures by scanning tunneling microscopy. At room temperature, small Se clusters are randomly dispersed on the surface. Increasing the temperature up to 200 °C, a well-ordered lattice of Se molecules consisting of 8 Se atoms in ring-like structure is formed. Further increasing the temperature to 250 °C gives rise to the formation of Se monolayer with Au(111)-$\sqrt{3}\times\sqrt{3}$ lattices superimposed with a quasi-hexagonal lattice. Desorption of Se atoms rather than the reaction between the Se atoms and the Au substrate occurs if further increasing the temperature. The ordered structures of selenium monolayers could serve as templates for self-assemblies and our findings in this work might provide insightful guild for the epitaxial growth of the two-dimensional transition metal dichalcogenides.

Keywords: STM, adsorption, selenium, structure transitions

PACS: 68.37.Ef, 68.43.–h, 74.62.–c **DOI:** 10.1088/1674-1056/ab821d

1. Introduction

Adsorption of chalcogen atoms on metal surfaces has been extensively studied for both the fundamental research and industrial applications. For instance, the chalcogen atoms serve as the headgroups of alkanethiol,[1] arenethiol,[2] alkanedithiol,[3] and dialkyldisulfide,[4] guiding the self-assembly process on metal surfaces and thus the formation of self-assembled monolayers of the linked organic molecules. In addition, the electronic properties of the metal surfaces can be tuned by the adsorption of the chalcogen atoms.[5] Besides, a thick layer of chalcogen is widely used as a capped layer to protect its subsequent surfaces or materials from exposure to air or other contaminations due to their inertness and relatively low evaporation temperature. For instance, adlayer of selenium can protect selenium-based superconductors like FeSe,[6] topological insulators like Bi_2Se_3,[7] and semiconductors like $MoSe_2$[8] from contaminations when exposing to air. Clean surfaces of these materials can be restored by simply annealing at modest temperature in vacuum. Further, two-dimensional transition metal dichalcogenides (2D TMDs) have attracted intensive interest in very recent years.[9–19] One unit layer of TMDs has three atomic layers, where the transition metal atom is sandwiched between two chalcogens. Diverse electronic properties of TMDs can be achieved by choosing different combinations of transition metal and chalcogen elements, giving rise to the formation of different phases.[20] A single layer of TMDs can have different phases depending on the stacking sequence of the three atomic layers, *e.g.*, trigonal prismatic phase and/or octahedral phase. Typically, only one of these two phases is thermodynamically stable in transition metal dichalcogenides. The phase engineering has been developed to change TMDs from one phase to different phases as well as the electronic properties.[20] To control the growth of the selective synthesized TMDs phase, it is important to tune the growth process thermodynamically and kinetically.[21,22] The growth phase of the transition metal dichalcogenides strongly depends on the amount and structures of the pre-treated chalcogen atoms on the substrate as well as the substrate temperature. However, the structural evolution of this buffered chalcogen layers with substrate temperature has been rarely reported, although the adsorption of chalcogen atoms on various substrates [like Au(111), Au(100), and Ag(111)] has been investigated in the past decades.[5,23–26] In most of these works, the chalcogen atoms were deposited onto the substate via chemical deposition in solutions, which inevitably involves some contamination or oxidation and thus affects the structures and electronic properties of the formed chalcogen layers. Thus, *in-situ* study of the growth behavior and structural evolution of the chalcogen layers under a clean environment is highly desired. In the present study, we investigate the growth behavior and structural evolution of selenium monolayers on Au(111) substrate at various temperatures by low-temperature scanning tunneling microscopy/spectroscopy (LT-STM/STS) under ultra-high vacuum (UHV) condition.

*Project supported by the Direct Grant for Research of CUHK, China (Grant Nos. 4053306 and 4053348).
†Corresponding author. E-mail: ydque@phy.cuhk.edu.hk
‡Corresponding author. E-mail: xdxiao@phy.cuhk.edu.hk
© 2020 Chinese Physical Society and IOP Publishing Ltd

2. Methods

2.1. Sample preparation

A clean Au(111) (MaTeck GmbH) surface was prepared by several cycles of Ar^+ ion sputtering ($P_{Ar} = 3 \times 10^{-5}$ mbar (1 bar = 10^5 Pa), 600 eV, 20 min) and subsequent annealing (450 °C, 10 min). The cleanness of Au(111) was verified by STM topographic images. The Se atoms/molecules were deposited onto the clean Au(111) surface via a home-made Knudsen cell heated at 140 °C. During deposition, the Au(111) substrate was kept at room temperature or elevated temperature (range from 200 °C to 400 °C), which is specified in the following text. The substrate temperature was measured by a K-type thermocouple welded to the heating stage next to the sample. Thus, the true substrate temperature might be somewhat lower than the measured values.

All the experiments were carried out in a UHV LT-STM system with a base pressure better than 2×10^{-10} mbar. The sample was directly transferred to the STM without breaking the UHV environment after the growth of Se films on Au(111) substrate.

2.2. STM/STS measurement

The STM images were acquired in a constant-current mode at the temperature of liquid nitrogen (~ 78 K) using an electrochemically etched tungsten tip and all the labelled bias voltages referred to the sample against tip. The dI/dV spectra were obtained by numerical differentiation of I–V spectra. Prior to the spectroscopic measurement, the STM tip was calibrated against the surface states of Au(111) or Cu(111) surface.

3. Results and discussion

The vapor phases of elemental selenium consist Se chains and ring-like Se_n-molecules.[27,28] Indeed, the deposition of Se on Au(111) at room temperature leads to the formation of Se clusters and Se short chains on the surface randomly, as shown in Fig. 1(a). For the individual Se clusters, it shows similar size and apparent STM height [~ 1 nm in width and ~ 1.4 Å in height, see Fig. 1(b)], indicating that the Se clusters might contain the same number of Se atoms. Beside the individual Se clusters, Se short chains are also found on the surface, due to the coalescence of the individual Se clusters. Both the STM image [Fig. 1(a)] and height profile [Fig. 1(b)] show the larger apparent STM height for the Se short chains compared to the individual Se clusters.

Increasing the Au(111) substrate temperature, the deposition of Se leads to the formation of uniform monolayer of Se. Figure 2(a) presents a typical STM topographic image of Se monolayer formed at 200 °C. It shows striped structures with two orientations as denoted by regions I and II (see the zoomed-in image in the inset). Two sets of spots are found in the fast Fourier-transformation (FFT) image shown in Fig. 2(b), which correspond to the striped structures with different orientations in Fig. 2(a). In the zoom-in STM image of region II [Fig. 2(c)], it reveals the 2D well-ordered array of squared structures. The size of these squares was measured to be 5.2 Å–5.8 Å. These squares form a distorted square lattice with lattice constants of ~ 8.5 Å. The angle between the lattice vectors was measured to be 77°. The unit cell of the distorted square lattice is denoted by the blue parallelogram. Similar structures were reported in a previous work,[23] where the squares were assigned to the Se_8 molecules with eight Se atoms arranged in a square shape. In the Se_8 molecules, four Se atoms locate at the square corners, and another four Se atoms at the side centers. The Se-Se bond length in the Se_8 molecules is 2.6 Å–2.7 Å. Thus, it is reasonable to assign the squared structures observed in Fig. 2(c) to the Se_8 molecules. Accordingly, the atomic structure of the distorted square lattice could be sketched as in Fig. 2(e). This distorted square lattice is referred to Se_8 lattice in the following text.

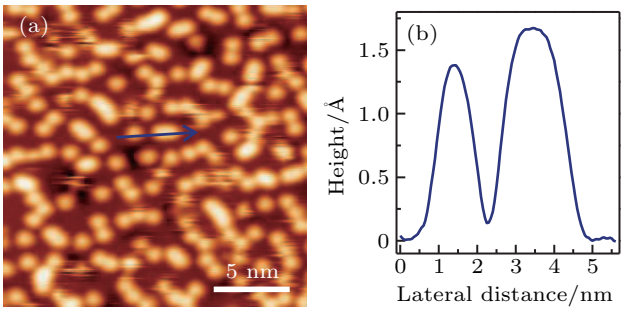


Fig. 1. Formation of Se clusters on Au(111) at room temperature. (a) STM image of Se/Au(111). (b) Height profile of Se clusters along the blue arrowed line in panel (a). The tunneling condition: $V_{bias} = -3.0$ V, $I_{set} = 50$ pA.

A superstructure is also found in Fig. 2(c) caused by the lattice mismatch as well as relative rotation between the substrate Au(111) lattice and the Se_8 lattice. The unit cell of the super lattice is indicated by the green parallelogram in Fig. 2(c). The lattice constant for the superstructure is ~ 2.2 nm, and the angle between the lattice vectors is ~ 77°. The FFT image presented in Fig. 2(d) shows two sets of patterns denoted by green triangles and blue circles, corresponding to the superlattices and Se_8 lattices respectively. The relationship between the superlattice and the Se_8 lattice can be written by the following transform matrix:

$$T = \begin{pmatrix} 2 & -2 \\ 1 & 2 \end{pmatrix}. \quad (1)$$

Integer numbers in the transform matrix (1) imply that the superstructure lattices are commensurate with Se_8 lattice.

Besides, the scanning tunneling spectroscopy (STS) was employed to investigate the electronic structures of the as-grown Se thin films on Au(111). Figure 2(f) presents the typical differential conductance spectrum of the Se_8 structures

formed on Au(111). Two small peaks at −0.3 V (red arrow) and −0.8 V (orange arrow) correspond to the Shockley state of Au(111) surface and the first onset valence band of the ring-like Se_8 structures, respectively. The rapid increase beyond 1 V above the Fermi level in the spectrum results from the conduction bands of the Se_8 structures.

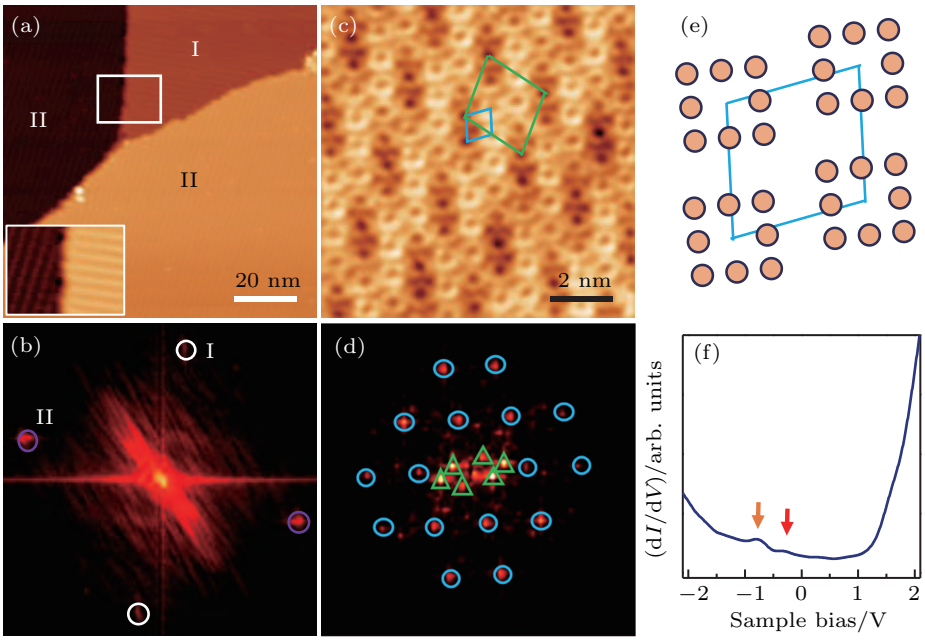


Fig. 2. Formation of Se ring-like structures on Au(111) at 200 °C. Large scale STM image (a) and the corresponding FFT image (b) of Se/Au(111). The inset is the zoomed-in image of the area indicated by the white rectangle. Zoomed-in STM image (c) of the region II in panel (a) and the corresponding FFT image (d) of Se/Au(111) in the region II in panel (a). (e) Schematic atomic structures of Se ring-like self-assembled thin film. (f) $\mathrm{d}I/\mathrm{d}V$ spectrum of the ring-like Se/Au(111). Tunneling conditions: (a) $V_{\mathrm{bias}} = 2.0$ V, $I_{\mathrm{set}} = 1.0$ nA; (c) $V_{\mathrm{bias}} = 1.0$ V, $I_{\mathrm{set}} = 500$ pA; (f) $V_{\mathrm{bias}} = 2.0$ V, $I_{\mathrm{set}} = 500$ pA.

Interestingly, further increasing the substrate temperature during the Se deposition gives rise to the formation of a totally different hexagonal Se structure. Figure 3(a) shows a large-area STM image of Se monolayer formed on Au(111) at 250 °C. It reveals a quasi-hexagonal superstructure similar to the superstructure in Si(111)-7 × 7 surface reconstruction, where each unit cell contains two triangular halves. In the Se superstructures [Fig. 3(a)], the upward halves are overall larger than the downward ones. These triangular halves vary in sizes over the surface, thus leading to less ordered superstructures. The corresponding FFT image of this superstructure shown in the inset of Fig. 3(a) shows a set of sharp spots in hexagonal pattern along with six branches, implying the quasi-hexagonal structures. The overall period for such quasi-hexagonal structure is ∼ 5.8 nm. In the atomic-resolution STM image, as shown in Fig. 3(b), it shows highly ordered hexagonal structures with lattice constant of ∼ 4.9 Å, $\sqrt{3}$ times of that of Au(111) (2.88 Å). Such Au(111)-$\sqrt{3} \times \sqrt{3}$ structures (referred as Se-$\sqrt{3}$ lattice) were also observed in previous work by low energy electron diffraction (LEED) and STM in the Se monolayer formed by electrodeposition.[23,24] In addition, it clearly shows the networks of the grain boundaries. Within the triangular grains, the nearest Se–Se distance is ∼ 4.9 Å, whereas crossing the boundaries, it ranges from 5.5 Å to 5.7 Å. Such much larger Se–Se distance compared with that in the Se_8 structure implies the deposited Se clusters/molecules were decomposed into individual Se atoms on Au surface at higher temperature during the deposition. Besides, it shows more defects in the corners connecting six neighboured grains. Thus, the formation of Se-$\sqrt{3}$ structure with networks of grain boundaries might the result of competition between the Se–Au and Se–Se couplings as well as defects or impurities on the surface. Figure 3(c) presents the FFT image of the atomically resolved STM image with larger area (25 nm × 25 nm, the same as Fig. 3(b) except for the larger scanning area). The six brighter outmost spots correspond to the hexagonal atomic lattices, whereas the inner sea-star shaped pattern same as the inset of Fig. 3(a) originates from the quasi-hexagonal super lattices. It is worth to note a transition from the Se_8 structure to Se-$\sqrt{3}$ structure by further annealing the Se monolayers with Se_8 structures at 250 °C, further confirming that the Se molecules are decomposed into individual Se atoms on Au surface. Thus, it is reasonable that these two Se adsorption structures coexist on the same sample at the substrate temperature between 200 °C and 250 °C.

Figure 3(d) presents the topographic image at 1.5 V for the same area shown in Fig. 3(b). It clearly shows the contrast differences in the two triangular halves in each unit cell. Such bias-dependent topographic images might originate from the electronic structures of the Se atoms in the two triangu-

lar halves. Indeed, the series of STS spectra crossing the two halves shown in Fig. 3(e) reveal the differences in the local density of states (LDOS) within the unit cells. Below the Fermi level, the spectra are almost the same with a peak around −0.7 V, corresponding the first onset valence band of the Se-$\sqrt{3}$ monolayer. Above the Fermi level, it shows two peaks at 1.7 V and 2.3 V for the downward triangular halve, corresponding to the first and second onset conduction band of the Se-$\sqrt{3}$ monolayer, whereas it shows a strong peak at 2.1 V with a small shoulder at 1.7 V for the upward triangular halve. Thus, lower LDOS at the upward triangular area gives rise to the darker contrast in the topographic image at 1.5 V. The change in the LDOS above the Fermi level might originate from the quantum confinement effects, since the two triangular halves have different areas.

Previous x-ray photoemission spectroscopic measurement on Se monolayers with Au(111)-$\sqrt{3} \times \sqrt{3}$ structures formed by electrodeposition reveals no chemical bond formation between the Se atoms and Au(111) substrate.[25] Therefore, the formation such Se monolayer implies no reaction between the Se atoms and the substrate under this moderate temperature, which is in consistence with the inertness of the noble metal gold. The question comes out: whether the reaction between and selenium and Au(111) could occur at higher substrate temperature and thus results in the formation of gold selenide.

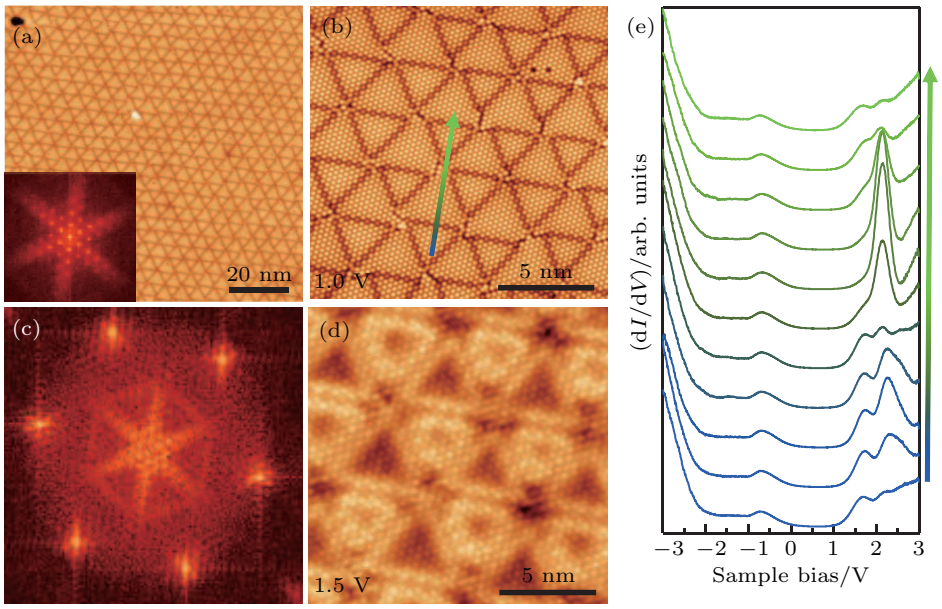


Fig. 3. Formation of Se-$\sqrt{3}$ monolayer on Au(111) at 250 °C. [(a), (b), (d)] Large-scale and atomic-resolution [(b), (d)] STM images of Se-$\sqrt{3}$ monolayer. The inset in panel (a) is the corresponding FFT image. (c) FFT image of the atomic-resolution STM image of Se-$\sqrt{3}$ monolayer with a scanning area of 25 nm × 25 nm. (e) Series of dI/dV spectra taken along the line indicated in panel (b). Tunneling conditions: (a) $V_{\rm bias} = -2.0$ V, $I_{\rm set} = 200$ pA; (b) $V_{\rm bias} = 1.0$ V, $I_{\rm set} = 500$ PA; (d) $V_{\rm bias} = 1.5$ V, $I_{\rm set} = 500$ pA; (e) $V_{\rm bias} = -2.0$ V, $I_{\rm set} = 500$ pA.

Figure 4 presents the typical STM topographic images for the Se nanostructures formed at higher substrate temperatures (300 °C and 400 °C). At 300 °C, it shows small patches of Se islands with different shapes and sizes with small gaps between these islands, as shown in Fig. 4(a). Within the small islands, the Se atoms are arranged in a hexagonal lattice with average lattice constant of ∼5 Å, the same as that in the Se-$\sqrt{3}$ lattice formed at 250 °C. In contrary, at 400 °C, it forms short Se chains with larger gaps between these chains [Fig. 4(b)]. The average Se–Se distance in the chains is around ∼5 Å. The gaps between these small islands or short chains implies the re-evaporation of Se atoms on the Au(111) surface at higher temperature, which is in consistent with the previous work.[26] Despite the gaps between the islands or chains, the Se atoms are arranged in the same way as Se monolayer with Se-$\sqrt{3}$ lattice, indicating no formation of gold selenide at such higher temperature. Further annealing the Se layers on Au formed at lower temperature to such higher temperatures gives rise to the same results as shown in Fig. 4.

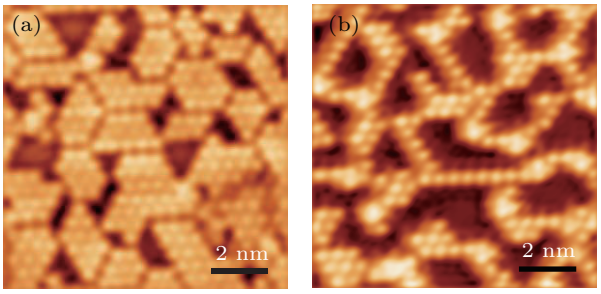


Fig. 4. Formation of Se structures on Au(111) at 300 °C (a) and 400 °C (b), respectively. Tunneling conditions: (a) $V_{\rm bias} = 0.5$ V, $I_{\rm set} = 1.0$ nA; (b) $V_{\rm bias} = -0.1$ V, $I_{\rm set} = 1.0$ nA.

4. Summary

In summary, we have systematically investigated the structures of the Se thin films formed on Au(111) at various

temperatures via STM. At room temperature, small Se clusters are randomly dispersed on the surface. Increasing the temperature up to 200 °C, well-ordered lattice of Se_8 molecules is formed. Further increasing the temperature to 250 °C gives rise to the formation of Se monolayer with Au(111)-$\sqrt{3}\times\sqrt{3}$ lattices superimposed with a quasi-hexagonal lattice. Desorption of Se atoms rather than the reaction between the Se atoms and the Au substrate occurs if further increasing the temperature. The ordered structures could serve as templates for the self-assemblies and our findings in this work might provide insightful guild for the epitaxial growth of the two-dimensional transition metal dichalcogenides.

References

[1] Guo Q and Li F 2014 *Phys. Chem. Chem. Phys.* **16** 19074

[2] Yang G, Qian Y, Engtrakul C, Sita L R and Liu G Y 2000 *J. Phys. Chem. B* **104** 9059

[3] Akkerman H B, Naber R C G, Jongbloed B, Van Hal P A, Blom P W M, De Leeuw D M and De Boer B 2007 *Proc. Natl. Acad. Sci. USA* **104** 11161

[4] Vericat C, Vela M E, Benitez G, Carro P and Salvarezza R C 2010 *Chem. Soc. Rev.* **39** 1805

[5] Lee M, Kang S, Oh M, Chae J, Yu J and Kuk Y 2019 *Surf. Sci.* **685** 19

[6] Zhang S, Guan J, Wang Y, Berlijn T, Johnston S, Jia X, Liu B, Zhu Q, An Q, Xue S, Cao Y, Yang F, Wang W, Zhang J, Plummer E W, Zhu X and Guo J 1955 *Phys. Rev. B* **97** 1

[7] Dai J, Wang W, Brahlek M, Koirala N, Salehi M, Oh S and Wu W 2015 *Nano Res.* **8** 1222

[8] Liu H, Zheng H, Yang F, Jiao L, Chen J, Ho W, Gao C, Jia J and Xie M 2015 *ACS Nano* **9** 6619

[9] Radisavljevic B, Radenovic A, Brivio J, Giacometti V and Kis A 2011 *Nat. Nanotechnol.* **6** 147

[10] Wang Q H, Kalantar-Zadeh K, Kis A, Coleman J N and Strano M S 2012 *Nat. Nanotechnol.* **7** 699

[11] Berghäuser G, Bernal-Villamil I, Schmidt R, Schneider R, Niehues I, Erhart P, de Vasconcellos S M, Bratschitsch R, Knorr A and Malic E 2018 *Nat. Commun.* **9** 971

[12] Lopez-Sanchez O, Lembke D, Kayci M, Radenovic A and Kis A 2013 *Nat. Nanotechnol.* **8** 497

[13] Ugeda M M, Bradley A J, Shi S F, Felipe H, Zhang Y, Qiu D Y, Ruan W, Mo S K, Hussain Z and Shen Z X 2014 *Nat. Mater.* **13** 1091

[14] Xu X, Yao W, Xiao D and Heinz T F 2014 *Nat. Phys.* **10** 343

[15] Jin Y, Keum D H, An S, Kim J, Lee H S and Lee Y H 2015 *Adv. Mater.* **27** 5534

[16] Xie L and Cui X 2016 *Proc. Natl. Acad. Sci. USA* **113** 3746

[17] Mouafo L D N, Godel F, Froehlicher G, Berciaud S, Doudin B, Kamalakar M V and Dayen J F 2016 *2D Mater.* **4** 15037

[18] Manzeli S, Ovchinnikov D, Pasquier D, Yazyev O V and Kis A 2017 *Nat. Rev. Mater.* **2** 17033

[19] Husain S, Kumar A, Kumar P, Kumar A, Barwal V, Behera N, Choudhary S, Svedlindh P and Chaudhary S 2018 *Phys. Rev. B* **98** 180404

[20] Voiry D, Mohite A and Chhowalla M 2015 *Chem. Soc. Rev.* **44** 2702

[21] Xu H, Han D, Bao Y, Cheng F, Ding Z, Tan S J R and Loh K P 2018 *Nano Lett.* **18** 5085

[22] Cheng F, Hu Z, Xu H, Shao Y, Su J, Chen Z, Ji W and Loh K P 2019 *ACS Nano* **13** 2316

[23] Lister T E and Stickney J L 1996 *J. Phys. Chem.* **100** 19568

[24] Sorenson T A, Lister T E, Huang B M and Stickney J L 1999 *J. Electrochem. Soc.* **146** 1019

[25] Jia J, Bendounan A, Kotresh H M N, Chaouchi K, Sirotti F, Sampath S and Esaulov V A 2013 *J. Phys. Chem. C* **117** 9835

[26] Nagashima S 1997 *Appl. Surf. Sci.* **121–122** 116

[27] Becker J, Rademann K and Hensel F 1991 *Z. Phys. D: At. Mol. Clust.* **19** 233

[28] Benamar A, Rayane D, Melinon P, Tribollet B and Broyer M 1991 *Z. Phys. D: At. Mol. Clust.* **19** 237